Archives of Biochemistry and Biophysics 606 (2016) 16–25

Contents lists available at ScienceDirect

Archives of Biochemistry and Biophysics

journal homepage: www.elsevier.com/locate/yabbi

Analysis of the pH-dependent thermodynamic stability, local motions, and microsecond folding kinetics of carbonmonoxycytochrome *c*

Rajesh Kumar [a, b, *]

[a] Centre for Chemical Sciences, School of Basic and Applied Sciences, Central University of Punjab, Bathinda, 151001, India
[b] School of Chemistry and Biochemistry, Thapar Institute of Engineering and Technology University, Patiala, 147004, India

ARTICLE INFO

Article history:
Received 12 March 2016
Received in revised form
11 June 2016
Accepted 13 July 2016
Available online 15 July 2016

Keywords:
Thermodynamic stability
Low-frequency local motion
Microsecond folding kinetics
Ionic interactions

ABSTRACT

This paper analyzes the effect of pH on thermodynamic stability, low-frequency local motions and microsecond folding kinetics of carbonmonoxycytochrome *c* (Cyt-CO) all across the alkaline pH-unfolding transition of protein. Thermodynamic analysis of urea-induced unfolding transitions of Cyt-CO measured between pH 6 and pH 11.9 reveals that Cyt-CO is maximally stable at pH~9.5. Dilution of unfolded Cyt-CO into refolding medium forms a native-like compact state (NCO-state), where Fe^{2+}–CO interaction persists. Kinetic and thermodynamic parameters measured for slow thermally-driven CO dissociation (NCO→N+CO) and association (N+CO→NCO) reactions between pH 6.5 and pH 13 reveal that the thermal-motions of M80-containing Ω-loop are decreased in subdenaturing limit of alkaline pH. Laser photolysis of Fe^{2+}-CO bond in NCO-state triggers the microsecond folding (NCO→N). The microsecond kinetics measured all across the alkaline pH-unfolding transition of Cyt-CO produce rate rollover in the refolding limb of chevron plot, which suggests a glass transition of NCO en route to N. Between pH 7 and pH 11.9, the natural logarithm of the microsecond folding rate varies by < 1.5 units while the natural logarithm of apparent equilibrium constant varies by 11.8 units. This finding indicates that the pH-dependent ionic-interactions greatly affect the global stability of protein but have very small effect on folding kinetics.

1. Introduction

The stability of proteins is generally governed by electrostatic [1–3], hydrophobic [4,5] and hydrogen bonding [6,7] interactions. However, the relative contributions of each of these interactions vary from one protein to another and also with the solution conditions under which protein is exposed [3,5]. Particularly, the ionic interactions in proteins seem to be very complex, sometimes favorable and sometimes unfavorable. The electrostatic interactions have great importance in protein structure and function [8,9]. The contributions of electrostatic interactions to protein stability are generally determined by evaluating the thermodynamic stability of protein as a function of pH [9–11]. In general, pH modulates the thermodynamic stability of proteins by altering the charges on ionizable groups. A number of previous studies indicate that the ionic interactions among the charged residues play important roles in protein folding and stability [8,12–15]. Apart from the stability of native proteins, the ionic interactions also play significant role in the folding pathway. Two recent pH-dependent theoretical and experimental studies on prion protein have revealed that the extreme acidic pH can misfold the prion protein which could refold again by enhancing the pH back to 7 [16–18].

The pH-dependence of stability [9–11,19–40] and millisecond folding kinetics of proteins have been widely investigated [9–11,36–40]. However, the pH-dependence of internal dynamics and microsecond folding dynamics of proteins have received less attention [41,42]. The present work analyzes the effect of pH on thermodynamic stability, low-frequency local motions (*i.e.,* thermal collisions due to collective motional mode of the M80-containing Ω-loop) and microsecond folding kinetics of Cyt-CO all across the alkaline pH-unfolding transition of protein. The present work also estimates the development of electrostatic interactions in the transition state for folding of Cyt-CO. Cytochrome *c* (Cyt *c*) is primarily known as an electron-carrying mitochondrial heme protein that also involves in initiation of apoptosis. Upon release of Cyt *c* to the cytoplasm, the protein binds apoptotic protease activating

* Centre for Chemical Sciences, School of Basic and Applied Sciences, Central University of Punjab, Bathinda, 151001, India.
E-mail address: rajeshchem01@gmail.com.

http://dx.doi.org/10.1016/j.abb.2016.07.010
0003-9861/

factor-1 (Apaf-1). The clusters of anionic and cationic residues on Cyt *c* play an important role in binding of Cyt *c* to cyt oxidase, cyt reductase and other components of electron transfer chain [43,44]. An earlier report showed that the (de)protonations of ionic residues due to the change in pH of mitochondrial intermembrane space influence the binding efficacy of Cyt *c* to these components, which in result alter the normal function of Cyt *c* and thus induce the apoptosis [45].

The axial ligands of heme iron in native ferrocytochrome *c* (Ferrocyt *c*) are H18 and M80. Furthermore, the binding of alternative ligands is strongly disfavored under physiological conditions [46]. However, CO and other exogenous ligands have such a strong affinity for binding with Fe^{2+} of heme that they can displace the native M80 ligand under partially denaturing conditions [47–52]. Cyt-CO continues to be a standard model for protein folding and dynamics studies [47–52]. The dilution of unfolded Cyt-CO into native buffer results in the collapse and formation of native-like compact state (NCO-state) [48–50]. NCO-state preserves the non-native Fe^{2+}–CO contact and exhibits the generic properties of molten globules (MGs) [48–50]. Pulsed laser photolysis of the CO ligand in NCO-state triggers the microsecond folding (NCO→N) [48–50]. Thermal-fluctuations of the M80-containing Ω-loop control the slow thermally-driven CO dissociation (NCO→N+CO) and association (N+CO→NCO) reactions [51,52]. Analysis of pH-dependent thermal-fluctuations and microsecond folding kinetics of NCO reveals that (i) thermal-motions of Ω-loop are decreased in subdenaturing limit of alkaline pH, and (ii) NCO→N folding proceeds *via* at least one glassy state.

2. Materials and methods

2.1. Chemicals and protein

Horse heart cytochrome *c* (Cyt *c*) (type VI) and all other chemical were purchased from Sigma. All equilibrium and kinetic experiments of Cyt-CO were carried out in a mixer of buffers (10 mM of each Tris, disodium hydrogen phosphate and CAPS (3-[Cyclohexylamino]-1-propanesulfonic acid) under controlled anaerobic atmosphere.

2.2. Equilibrium unfolding measurements

Cyt *c* samples were prepared in 0–11.0 M range of urea. For equilibrium unfolding measurement of Ferrocyt *c*, Cyt *c* samples containing different concentrations of urea were deaerated by using dry nitrogen gas and reduced by using freshly prepared sodium dithionite solution. Cyt-CO samples were prepared by purging dry CO gas into freshly prepared Ferrocyt *c* samples for a minute. Prior to fluorescence measurements, Ferrocyt *c* and Cyt-CO samples were incubated for an hour at 25 °C. Fluorescence emission spectra (excitation: 280 nm, emission: 310–410 nm) were measured at 25 °C using a FluoroMax-3 instrument (Jobin-Yvon, Horiba). The final concentrations of reductant and protein were ~3 mM and 12 μM, respectively. The concentrations of the urea solutions were measured on the basis of refractive index (Abbe refractometer). The final concentrations of urea are those measured after experiments.

2.3. Measurement of pH-titrations of Ferrocyt c both in the absence and presence of CO

Cyt *c* samples were prepared in a mixer of buffers. pH of protein samples were adjusted from pH 7 to pH 13.5 by using concentrated NaOH. These protein samples were deaerated using dry N_2 gas and reduced by adding freshly prepared sodium dithionite solution under strict anaerobic atmosphere. For measurement of pH titration of Cyt-CO, dithionite-reduced protein samples were saturated with CO by passing a slow stream of dry CO gas through solution for a minute. Protein samples were incubated for ~40 min in tightly capped glass tubes at 25 °C. Fluorescence emission (excitation: 280 nm, emission: 310–410 nm) and optical absorption (380–750 nm) spectra were recorded at 25 °C. The final concentrations of sodium dithionite and protein were ~3 mM and ~12 μM, respectively. The final pH of protein samples were those measured after experiments. pH titration curves of Cyt-CO were analyzed by using the transformed Henderson-Hasselbalch equation (eq (1)) [53],

$$Y_{obs} = \frac{A + B\left[10^{n(pH-c_m)}\right]}{1 + 10^{n(pH-c_m)}} \quad (1)$$

where, *A* and *B* are the normalized spectroscopic signals for the denatured and folded states, respectively, C_m is pH denaturation midpoint, and *n* is the number of OH^- ions titrated during transitions.

2.4. Measurement of far-UV CD spectra of Cyt-CO

Urea-unfolded Cyt-CO (UCO) was prepared by passing the dry CO gas into Ferrocyt *c* containing ~10.5 M urea at pH 7 under N_2 atmosphere. UCO was diluted into degassed and dithionite reduced CO-free buffers between pH 7 and pH 13. This procedure allows refolding of UCO to NCO between pH 7 and pH 12. However, above pH 12.5, UCO remains unfolded. The far-UV CD spectra of NCO-state between pH 7 and pH 13 were recorded on Jasco 810 CD spectrophotometer.

2.5. Measurement of ^{1}H NMR spectra of Cyt-CO

Base-unfolded Cyt-CO (UCO) was prepared by passing dry CO gas into alkaline Ferrocyt at pH 13 under N_2 atmosphere. UCO (pH 13) was diluted into degassed and dithionite reduced buffer at pH 6, 7.5 and 13. This procedure allowed refolding of UCO to NCO at pH 6 and 7.5 but at pH 13, UCO remains unfolded. After dilution of UCO (pH 13) into pH 6 and pH 7.5 buffers, the pH of these buffers drifted from 6 to 7.5 and 7.5 to 10.7. The ^{1}H NMR spectra of NCO at pH 7.5 and 10.7 and UCO at pH 13 were recorded on JEOL 400 MHz spectrometer.

2.6. Preparation of the NCO-state and measurement of CO dissociation kinetics

Unfolded Cyt-CO (UCO) was prepared by CO ligation to unfolded Ferrocyt *c* at pH 7 under N_2 atmosphere. NCO-state was prepared by about 100 fold dilution of UCO into a desired pH deaerated and dithionite-reduced CO-free refolding buffer. The fast UCO→NCO process subsequently follows the slow thermally-driven NCO→N+CO dissociation. CO dissociation kinetics was measured by heme absorbance (550 nm) at 22 °C. For CO dissociation kinetic experiments, the final concentrations of protein and sodium dithionite were ~10 μM and ~3 mM, respectively.

2.7. Measurement of CO association kinetics

CO-association kinetics was performed with the same method as described previously [52]. Briefly, ~20 μl solution of Ferrocyt *c* (1 mM, pH 7) was mixed rapidly with a 2 ml of CO-saturated buffer of a desired pH containing ~2.5 mM sodium dithionite. CO association kinetics was measured by heme absorbance (550 nm) at 22 °C. For CO association kinetic experiments, the final concentrations of protein and sodium dithionite were ~10 μM and ~3 mM,

respectively.

2.8. Measurement of millisecond refolding kinetics of UCO-state

Cyt *c* was dissolved in a mixer of buffers that contained 5 M GdnHCl and 0.5 M NaCl. The pH of unfolded protein sample was adjusted to 7 and 12.8 and deaerated by using dry N_2 gas. These proteins samples were reduced by adding freshly prepared sodium dithionite solution under strict anaerobic atmosphere. Unfolded Cyt-CO (UCO) was prepared by CO-ligation to Ferrocyt *c* (5 M GdnHCl) under N_2 atmosphere. While urea is a better denaturant for electrostatic interaction studies [11,24] but for the millisecond refolding studies of Cyt-CO, UCO was prepared by CO-ligation to Ferrocyt *c* in 5 M GdnHCl than in 10 M urea because CO-ligation to Ferocity *c* is a denaturation reaction (since the very stable intrinsic native Fe^{2+}- M80 bond is broken, creating a 5-coordinate heme capable of binding CO) and which occurs faster in 5 M GdnHCl than in 10 M urea [51-52]. UCO samples thus prepared at pH 7 and 12.8 were refolded by stopped-flow dilution in 50 mM phosphate buffer (pH 7, 0.5 M NaCl) and in 20 mM CAPS buffer (pH 11.7, 0.5 M NaCl), respectively. The final concentrations of protein, sodium dithionite and GdnHCl in refolding buffer were ~15 μM, ~3 mM and 0.8 M, respectively. The refolding kinetics was measured using a SFM 400 mixing module (Biologic). Excitation wavelength was 280 nm and emission was measured using a 358 nm cut-off filter at pH 7 and 335 nm cut-off filter at pH 12.8. Typically, 7-8 shots were averaged.

2.9. Measurement of microsecond folding kinetics of NCO-state

UCO was prepared with the same procedure as mentioned for the slow CO dissociation kinetics of NCO. The NCO-state was prepared by 25 fold dilution of UCO into a degassed and dithionite-reduced CO-free refolding buffer of desired pH. The NCO-state preserves the Fe^{2+}–CO contact for ~45 min at pH 7, 22 °C [52]. Single-pulse CO-photolysis experiments of NCO were completed within 1–3 min of preparation of NCO state. CO photolysis of NCO was carried out on a nanosecond flash photolysis apparatus (Applied Photophysics) by irradiation with 80 (±10) mJ pulses of the 532-nm second harmonic output of a Spectra Physics Q-switched Nd/YAG laser (10 Hz). Following the photolysis pulse, the spectral changes at 550 nm were recorded with a pulsed Xe lamp. A fresh sample was used for each single-pulse kinetic trace. For each pH sample, three to four kinetic traces were taken at 25 °C. The final concentrations of CO, sodium dithionite and protein were about 50 μM, 3 mM and 45 μM, respectively.

3. Results

3.1. pH-dependence of ΔG_D° and m_g of Cyt-CO

Native Cyt *c* is fluorescence-silent due to excitation energy transfer from lone W59 to the heme [54]. Unfolding results in increase of heme-tryptophan distance due to molecular expansion [54,55]. Fig. 1a presents the W59 fluorescence-monitored normalized urea-induced equilibrium unfolding transitions of Cyt-CO measured at several different pH values, ranging from 6 to 11.9. To assess the effect of pH on thermodynamic stability of Cyt-CO, these urea-induced unfolding curves of Cyt-CO (Fig. 1a) were analyzed using the standard two-state equation (eq (2)) [56],

$$Y_{obs} = \frac{(\alpha_N + m_N[D]) + (\alpha_U + m_U[D])\exp\left[\frac{-\Delta G_D^\circ + m_g[D]}{RT}\right]}{1 + \exp\left[\frac{-\Delta G_D^\circ + m_g[D]}{RT}\right]} \quad (2)$$

The resulting unfolding free energy (ΔG_D°) and surface area exposed by the solvent (m_g) are provided in Table 1. Fig. 1b shows the pH dependence of ΔG_D°. As pH is increased from 6 to 11.9, the ΔG_D° initially increases and reaches a maximum at pH ~9.5 and then decreases (Fig. 1b). The pH dependence of m_g is shown in Fig. 1c. The m_g value does not change greatly up to pH ~11.9 (Fig. 1c).

3.2. pH titrations of Ferrocyt c and Cyt-CO

Fig. 1d shows the normalized tryptophan fluorescence-monitored pH-titration curves of Ferrocyt *c* and Cyt-CO at 25 °C. The data in Fig. 1d revealed that within the pH range from 7 to 13.5, Ferrocyt *c* possesses structural integrity very similar but Cyt-CO almost denatured at pH > 12.6. Previous NMR studies of alkaline Ferrocyt *c* and Cyt-CO also showed that the secondary and tertiary structural contents of alkaline Ferrocyt *c* (pH 12.7) are very similar to native Ferrocyt *c* (pH 7) but Cyt-CO almost denatured at pH ~12.7 [57,58]. Fig. 1d also shows the normalized visible absorbance (550 nm)-monitored pH-titration curve of Cyt-CO at 25 °C. Data in Fig. 1d clearly suggested that the absorbance monitored CO-induced unfolding transition shifts to lower pH, relative to that measured by fluorescence (CO-induced unfolding pH-midpoints for the absorbance and fluorescence-monitored pH-titrations are ~11.8 and 12.4, respectively).

3.3. pH-dependence of log k_{ass} and log k_{diss}

Fig. 2a presents the steady-state visible absorption spectra of NCO and N-states collected at pH 7 (22 °C). Fig. 2b and c show the influence of pH on kinetics of CO dissociation and association reactions, respectively at 22 °C. CO dissociation kinetic data in Fig. 2b are best described by a single-exponential rate expression with rate constant, k_{diss} ~6.9 × 10^{-4} s^{-1}, ~2.8 × 10^{-4} s^{-1} and ~2.7 × 10^{-3} s^{-1} at pH ~7, 11 and 12.9, respectively. Clearly, as pH is increased from 7 to 11, k_{diss} decreases by ~2.5 fold. CO association kinetic data in Fig. 2c are also best described by a single-exponential rate expression with rate constant, k_{ass} ~8.4 × 10^{-4} s^{-1}, ~3.2 × 10^{-4} s^{-1} and ~3.8 × 10^{-2} s^{-1} at pH ~7, 9.8 and 12.9, respectively. Upon increasing pH from 7 to 9.8, k_{ass} decreases by ~2.7 fold. On contrary, when pH is increased from 7 to 12.9, k_{diss} and k_{ass} increase by ~3.9 and ~44 folds, respectively.

Fig. 2d presents the pH dependence of log k_{ass} and log k_{diss}, which suggests "chevron-like" features for log k_{ass}-pH and log k_{diss}-pH space. Data in Fig. 2d clearly indicate that above pH 9, log k_{ass} and log k_{diss} are not superimposable, indicating that different mode of motions operates in CO association and dissociation processes. This finding is not surprising because CO association occurred with native state (N-state) while CO dissociation occurred from an artificially generated native-like highly compact state (NCO-state). As pH is raised from 6.5 to 13, log k_{ass} and log k_{diss} initially decrease up to pH ~9.8 and pH ~11, respectively and then increase (Fig. 2d). The decrease in log k_{ass} and log k_{diss} in subdenaturing limit of alkaline pH can be interpreted to arise from protein stabilization that would retard CO dissociation and association processes. Notably, relative to pH 7, log k_{ass} is found to be most decreased (Fig. 2d) near the pH where Cyt-CO has maximum thermodynamic stability (Fig. 1b and Table 1) and least CO affinity for active protein site (apparent dissociation constants, K_d at pH 7, 9.8 and 12.9 are ~580, ~710 and ~62 μM, respectively) (Inset of Fig. 2d). The increase in log k_{ass} and log k_{diss} under strongly alkaline pH conditions can be interpreted to arise due to protein destabilization and structural unfolding that would accelerate the CO association and dissociation processes.

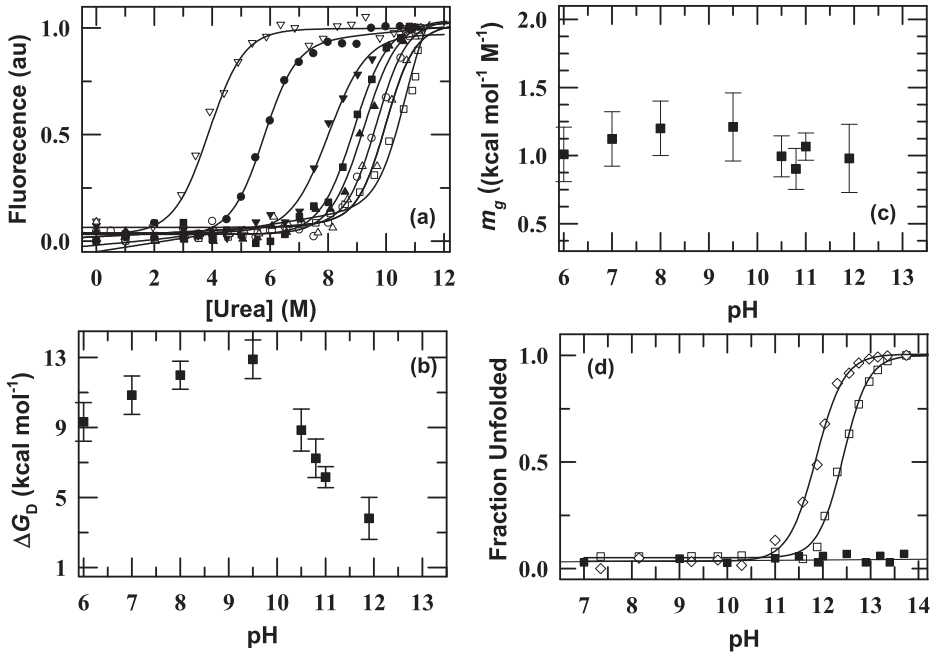

Fig. 1. pH-dependent stability of Cyt-CO. (a) Fluorescence monitored normalized urea-induced unfolding curves of Cyt-CO measured at pH 6.0 (▲), pH 7 (○), pH 8 (△), pH 9.5 (□), pH 10.5 (■), pH 10.8 (▼), pH 11 (•), and pH 11.9 (∇). The solid curves in panel (a) represent nonlinear least-squares fit using the standard two-state equation [56]. (b) pH dependence of ΔG_D° at 25 °C. (c) pH dependence of m_g at 25 °C. (d) Tryptophan fluorescence-monitored normalized pH-titrations of Ferrocyt *c* (■) and Cyt-CO (□) measured at 25 °C. Cyt-CO gets unfolded at pH > 12.7 (□) but there is no unfolding in case of Ferrocyt *c* (■). Panel (d) also presents the heme absorption (550 nm)-monitored normalized pH-titration of Cyt-CO (◊) measured at 25 °C. The solid lines in panel (d) are fit according to transformed Henderson-Hasselbalch equation [53].

Table 1
ΔG_D°, m_g, and C_m values for urea-induced unfolding of Cyt-CO monitored by Trp fluorescence (ex: 280 nm).

pH	ΔG_D°	m_g	C_m	pH	ΔG_D°	m_g	C_m
6	9.3(±1.1)	1.01(±0.2)	9.24	10.5	8.9(±1.2)	0.99(±0.1)	8.90
7	10.8(±1.1)	1.12(±0.2)	9.66	10.8	7.2(±1.1)	0.90(±0.2)	8.03
8	12.0(±0.8)	1.20(±0.2)	9.99	11.0	6.2(±0.6)	1.06(±0.1)	5.79
9.5	12.9(±1.1)	1.21(±0.2)	10.65	11.9	3.8(±1.2)	0.97(±0.2)	3.89

*ΔG_D°, m_g, and C_m are reported in kcal mol^{-1}, kcal mol^{-1} M^{-1}, and M, respectively. The uncertainty (standard error) is indicated in parenthesis.

3.4. pH-dependence of activation thermodynamic parameters

Fig. 3a presents the Eyring plots for CO dissociation reaction obtained from temperature dependent kinetic data at pH 7, 11 and 12.9. The Eyring plots for CO association reaction obtained from temperature dependent kinetic data at pH 7, 9.8 and 12.9 are shown in Fig. 3b. To find out the pH dependency of activation enthalpy ($\Delta H^{\ddagger}_{ass/diss}$) and activation entropy ($\Delta S^{\ddagger}_{ass/diss}$) for CO dissociation and association reactions, the Eyring plots in Fig. 3a and b were analyzed by eq (3) [59],

$$\ln(k_{ass/diss}h/k_BT) = (\Delta S^{\ddagger}_{ass/diss}/R) - (\Delta H^{\ddagger}_{ass/diss}/RT) \quad (3)$$

Tables 2 and 3 summarize the effect of pH on activation enthalpy, activation entropy and activation free energy for CO association and dissociation reactions. The data in Tables 2 and 3 provide some important information, (i) relative to pH 7, $\Delta H^{\ddagger}_{ass}$ and $\Delta H^{\ddagger}_{diss}$ increase at pH ~9.8 and ~11, respectively, which suggest that some additional internal attractive interactions in N- and NCO-states were originated in subdenaturing limit of alkaline pH which in result block the CO association and dissociation processes, (ii) the increase of $\Delta H^{\ddagger}_{ass/diss}$ is accompanied by a decrease in the entropy change $-T\Delta S^{\ddagger}_{ass/diss}$, and (iii) the enthalpic effect is more dominated than the entropic one.

3.5. pH dependence of millisecond folding kinetics of Cyt-CO

In stopped flow experiments (dead time ~2.5 ms), the dilution of GdnHCl-unfolded Cyt-CO (UCO-state) into native buffer at pH 7 refolds rapidly UCO-state to NCO-state [48–50]. Fig. 4a and b show the refolding kinetic profiles for UCO→NCO conformational transition measured at pH 7 and 11.9, respectively. These refolding kinetic data are best described by a two-exponential rate expression with rate constants, $k_{f1} \approx 310$ s^{-1} and $k_{f2} \approx 50$ s^{-1} at pH 7 (Fig. 4a) and $k_{f1} \approx 145$ s^{-1} and $k_{f2} \approx 15$ s^{-1} at pH 11.9 (Fig. 4b). About ten percent of the observed amplitude was due to slower minor phase which was probably due to fraction of oxidized protein. It is to be noted that between pH 7 and pH 11.9, the activation folding energy barrier ($\Delta G_D^{\circ\ddagger} = -RT\ln(hk_f/k_BT)$) of the protein varied less than by 0.5 kcal mol^{-1} ($\Delta G_D^{\circ\ddagger}$ values were ~10.7 and 11.2 kcal mol^{-1} at pH 7 and 11.9, respectively) while the folding energy barrier (ΔG_D°) which was measured by equilibrium denaturation experiments of Cyt-CO varied by 10.1 kcal mol^{-1} (ΔG_D° values were ~11.9 and 1.8 kcal mol^{-1} at pH 7 and pH 11.9, respectively) (Fig. 1b and Table 1). This finding clearly indicates that the large difference in thermodynamic stability of Cyt-CO at pH 11.9 relative to pH 7 is not strongly reflected in the refolding rates.

3.6. pH dependence of microsecond folding kinetics of Cyt-CO

Laser T-jump methods have been vastly used to capture the ultrafast folding events for a number of peptides and proteins [60,61]. When photolysed by light pulse ($h\nu$), photodissociation of CO of the Fe^{2+}-CO bond in NCO-state triggers folding [48–50]. Fig. 4c presents single pulse CO-photolysis triggered microsecond folding kinetic profiles for NCO→N transition measured for 25 μM and 50 μM protein at pH 7, 25 °C. CO photolysed kinetic data are

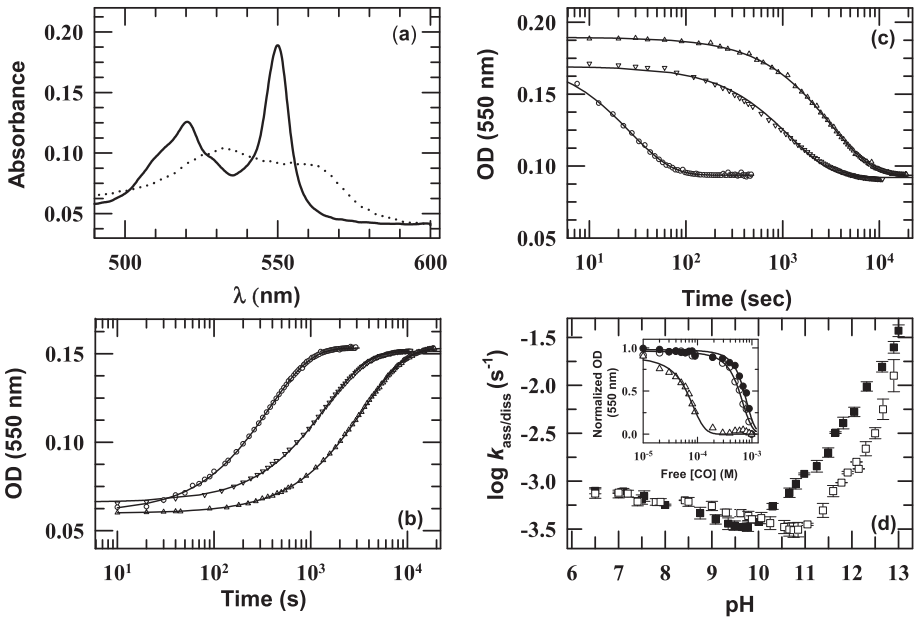

Fig. 2. (a) Steady-state visible absorption spectra of NCO (dashed line) and N (solid line) states measured at pH 7, 25 °C. The NCO→N reaction was probed at 550 nm, the λ_{max} of the N-state spectrum. Panel (b) presents representative kinetic traces for CO dissociation (NCO→N+CO) at pH 7 (∇), pH 11 (Δ) and pH 12.9 (o), 22 °C. The kinetic data for CO dissociation (panel (b)) were best described by mono-exponential rate expression with k_{diss} ~6.9×10^{-4} s^{-1}, ~2.8×10^{-4} s^{-1} and ~2.7×10^{-3} s^{-1} at pH 7, pH 11 and pH 12.9, respectively. Panel (c) presents representative kinetic traces for CO association (N+CO→NCO) reaction at pH 7 (∇), pH 9.8 (Δ) and pH 12.9 (o), 22 °C. The kinetic data for CO association (panel (c)) were also best described by mono-exponential rate expression with k_{ass} ~8.4×10^{-4} s^{-1}, ~3.2×10^{-4} s^{-1} and ~3.8×10^{-2} s^{-1} at pH 7, pH 9.8 and pH 12.9, respectively. (d) pH-dependence of the rates of CO association, k_{ass} (■) and dissociation, k_{diss} (□) at 22 °C. The inset of panel (d) shows the CO titration of Ferrocyt *c* recorded at pH 7 (O), 9.8 (•) and 13 (Δ), 22 °C. Fits to data are according to the equation $y(x) = 1/[1 + 10^{n(x-K)}]$, where x is the free CO concentration in reaction medium.

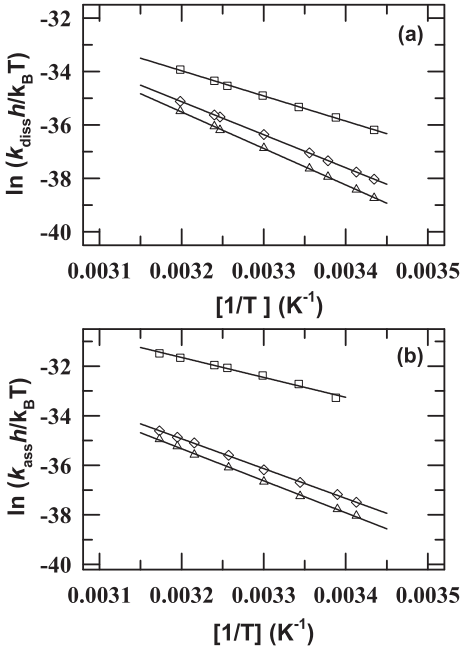

Fig. 3. (a) Eyring plots for CO dissociation reaction obtained from temperature-dependent kinetic data at pH 7 (◊), pH 11 (Δ) and pH 12.9 (□). (b) Eyring plots for CO association reaction obtained from temperature-dependent kinetic data at pH 7 (◊), pH 9.8 (Δ) and pH 12.9 (□). The activation enthalpies and activation entropies derived from linear least-squares fitting of Eyring plots for k_{diss} (panel (a)) and k_{ass} (panel (b)) values (solid line) are summarized in Tables 2 and 3.

best described by a single exponential rate expression with rate constant, $k_f \approx 2.66 \times 10^5$ s^{-1} ($\tau = 3.8$ μs) for 25 μM protein and $k_f \approx 2.3 \times 10^5$ s^{-1} ($\tau = 4.3$ μs) for 50 μM protein at pH 7.0, 25 °C. According to few previous studies, following CO photolysis from

Table 2
pH-dependence of $\Delta H^{\ddagger}_{ass}$, $\Delta S^{\ddagger}_{ass}$, $-T\Delta S^{\ddagger}_{ass}$, and $\Delta G^{\ddagger}_{ass}$ for CO association reaction.

pH	$\Delta H^{\ddagger}_{ass}$	$\Delta S^{\ddagger}_{ass}$	$-T\Delta S^{\ddagger}_{ass}$	$\Delta G^{\ddagger}_{diss}$
7	24.1(±0.2)	7.2(±0.5)	−2.1 (±0.1)	22.0 (±0.05)
9.8	26.0(±0.3)	12.0 (±1)	−3.6(±0.3)	22.4(±0.01)
12.9	16.0(±0.5)	−11.9 (±1.5)	3.5 (±0.4)	19.5(±0.05)

*$\Delta H^{\ddagger}_{ass}$, $\Delta S^{\ddagger}_{ass}$,$-T\Delta S^{\ddagger}_{ass}$, and $\Delta G^{\ddagger}_{ass}$ are reported as kcal mol^{-1}, cal $mol^{-1}K^{-1}$, kcal mol^{-1}, and kcal mol^{-1}, respectively. The uncertainty (standard error) is indicated in parenthesis.

Table 3
pH-dependence of $\Delta H^{\ddagger}_{diss}$, $\Delta S^{\ddagger}_{diss}$, $-T\Delta S^{\ddagger}_{diss}$, and $\Delta G^{\ddagger}_{diss}$ for CO dissociation reaction.

pH	$\Delta H^{\ddagger}_{diss}$	$\Delta S^{\ddagger}_{diss}$	$-T\Delta S^{\ddagger}_{diss}$	$\Delta G^{\ddagger}_{diss}$
7	24.7(±0.1)	8.9(±0.2)	−2.7 (±0.1)	22.0(±0.04)
11	27.4(±0.2)	16.4(±0.6)	−4.9(±0.2)	22.5(±0.02)
12.9	18.8(±0.3)	−7.5(±0.8)	2.3 (±0.2)	21.0(±0.06)

*$\Delta H^{\ddagger}_{diss}$, $\Delta S^{\ddagger}_{diss}$,$-T\Delta S^{\ddagger}_{diss}$, and $\Delta G^{\ddagger}_{diss}$ are reported as kcal mol^{-1}, cal $mol^{-1}K^{-1}$, kcal mol^{-1}, and kcal mol^{-1}, respectively. The uncertainty (standard error) is indicated in parenthesis.

base-denatured Cyt-CO (pH 13) [62,63] or GdnHCl-unfolded Cyt-CO (pH 7) [64–66], the side chains of the methionine (M65 and M80) and histidine (H26 and H33) residues make transient contacts with Fe^{2+} of heme. Fig. 4d shows the observed changes in 421 nm absorption from 70 ns to 30 μs after photodissociation of CO from the base-unfolded Cyt-CO (pH 13) in the absence of denaturant. The kinetic data are best fitted to a bi-exponential relaxation processes with rate constants, $\lambda_1 \approx 4.0 \times 10^6$ s^{-1} ($\tau_1 \approx 0.25$ μs) and $\lambda_2 \approx 5.2 \times 10^6$ s^{-1}($\tau_2 \approx 1.9$ μs). The fast ($\tau_1 \approx 0.25$ μs) and slow ($\tau_2 \approx 1.9$ μs) relaxation processes are related to the transient binding of the methionine (M65 and M80) and histidine (H26 and H33), respectively to the Fe^{2+} of photoproduct (Fig. 4d) [62–66].

Fig. 5a and Fig. 5b show the fluorescence and heme absorption

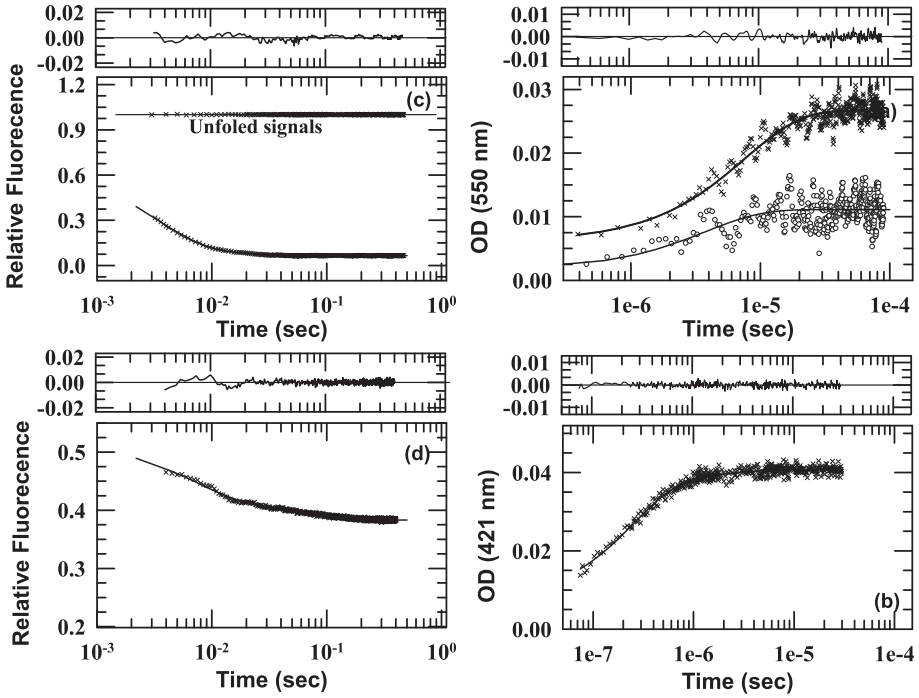

Fig. 4. Panels (a) and (b) show the stopped-flow refolding kinetic profiles for UCO→NCO transition measured at pH 7 and 11.9, respectively. These refolding kinetic data are best described by a two-exponential rate expression (residual shown) with rate constants, $k_{f1} \approx 310\ s^{-1}$ and $k_{f2} \approx 50\ s^{-1}$ at pH 7 (panel (a)) and $k_{f1} \approx 145\ s^{-1}$ and $k_{f2} \approx 15\ s^{-1}$ at pH 11.9 (panel (b)). (c) Representative single-pulse CO-photolysis-triggered microsecond folding kinetic traces of NCO (NCO→N folding) at pH 7.0, 25 °C, measured for 25 μM (○) and 50 μM (×) protein. The CO photolysed kinetic data for NCO→N folding transition is best described by a single exponential rate expression with rate constant, $k_f \approx 2.3 \times 10^5\ s^{-1}$ for 50 μM protein and $k_f \approx 2.66 \times 10^5\ s^{-1}$ for 25 μM protein. (d) Microsecond relaxation processes observed in heme optical absorption following photolysis of CO from base-unfolded Cyt-CO at pH 13, 25 °C. The kinetic data are best fitted to a bi-exponential relaxation processes (residual shown) with rate constants, $\lambda_1 \approx 4.0 \times 10^6\ s^{-1}$ ($\tau_1 \approx 0.25$ μs) and $\lambda_2 \approx 5.2 \times 10^6\ s^{-1}$($\tau_2 \approx 1.9$ μs).

(550 nm)-monitored pH-titration curves of Ferrocyt *c* and Cyt-CO, which clearly indicated that Cyt-CO was unfolded at pH ≥ 12.6 but pH ≥ 12.6, there was no unfolding in Ferrocyt *c*. This finding suggests that between pH 7 and pH 12.6, photodissociation of CO from NCO-state could trigger folding. The microsecond folding rate for NCO→N conformational transition was measured at sixteen different pH values, ranging from 7 to 12.6. The natural logarithm of the microsecond folding rate (ln k_f) is plotted as a function of pH in Fig. 5c. The microsecond relaxation rates (λ_1 and λ_2), measured after photodissociation of CO from base-unfolded Cyt-CO in the absence of denaturant at different pH values, ranging from 12.6 to 13.3, are also plotted as a function of pH in Fig. 5c. Notably, in the pre-transition region where NCO-state is most stable (pH < 11), ln k_f rolls over. The rollover of the rate at lower pH indicates that there is no pH dependence of the folding barrier below pH 11. When destabilizing conditions are approached (pH > 11), the rollover effect of ln k_f decreases rapidly (Fig. 5c). Above pH 12, ln k_f begins to increase and finally matches to the rates of microsecond relaxation processes measured by CO photolysis of base-unfolded Cyt-CO at pH 12.6. In the absence of denaturant, Cyt-CO is not fully unfolded at pH < 12.6. Due to this difficulty, the microsecond relaxation rates of base-unfolded cyt-CO were measured only at pH ≥ 12.6. Biphasic microsecond relaxation process following CO photolysis from unfolded Cyt-CO is the hallmark of heme-polypeptide diffusive dynamics [62–66], hence CO photolysis triggered microsecond rate for NCO→N conformational transition measured between pH 7 and pH 11 (Fig. 5c) contain the information related to the ultrafast folding kinetics. Furthermore, the linear extrapolation of ln k_f data from transition region to ordinate provides ln $k^\circ_{MN} \approx 16.2$, which correspond to $k^\circ_{MN} \approx 1.1 \times 10^7\ s^{-1}$ ($\tau \approx 0.1$ μs). The fastest folding rate observed here for NCO→N conversion ($k^\circ_{MN} \approx 1.1 \times 10^7\ s^{-1}$) very much matches to: (i) the rates of local hydrophobic collapse [67,68], (ii) the rate of tertiary conformational changes following laser photolysis of CO-bound heme proteins [69–73], and (iii) the folding rates of model peptide α-helix [74–77] and β-hairpin fragment [78].

3.7. *Δν analysis*

Comparison of pH-dependent stability profiles and pH-dependence of folding rates can provide the development of electrostatic interactions in the transition state for folding [9–11]. Between pH 7 and pH 11.9, ln k_f varied <1.5 units (Fig. 6a) while ΔG_D° decreased by 6.9 kcal mol^{-1} (Fig. 1b and Table 1) which correspond to a change in ln *K* by 11.8 units (Fig. 6b). This comparison demonstrates that the pH-dependent ionic interactions contribute significantly to thermodynamic stability of protein but have a very small effect on CO-photolysis induced microsecond folding kinetics of NCO. The classic Wyman-Tanford (WT) linkage relations can be used to relate the pH dependence of the apparent free energy of folding (ΔG°) and activation folding energy ($\Delta G^{\circ\ddagger}$) of protein [79,80].

$$\frac{\partial \Delta G^\circ}{\partial \mathrm{pH}} = 2.303RT\Delta\nu(\mathrm{pH}) \tag{4}$$

$$\frac{\partial \Delta G^{\circ\ddagger}}{\partial pH} = 2.303RT\Delta\nu^{\ddagger}(\mathrm{pH}) \tag{5}$$

where Δν(pH), and $\Delta\nu^{\ddagger}$(pH) are the differences in the number of protons bound to native and denatured states, and transition and unfolded states, respectively. The values of Δν (pH) between pH 6

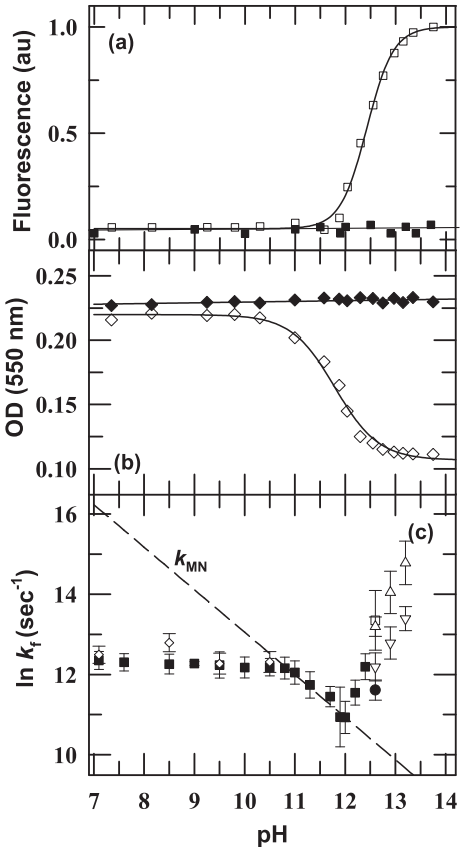

Fig. 5. (a) Fluorescence-monitored pH-titrations of Ferrocyt *c* (■) and Cyt-CO (□) at 25 °C. (b) Heme absorption (550 nm)-monitored pH-titrations of Ferrocyt *c* (◆) and Cyt-CO (◊) measured at 25 °C. The solid lines in panels (a) and (b) are fit according to transformed Henderson-Hasselbalch equation [53]. (c) pH-dependence of the microsecond folding rate (■) for NCO→N conformational transition at 25 °C for 25 μM (◊) and 50 μM (■) protein. Within the subdenaturing limit of alkaline pH (pH < 11), the ln k_f rolls over. As destabilizing conditions are approached (pH > 11), the rollover effect of ln k_f decreases rapidly. The linear extrapolation of the ln k_f data from transition region to ordinate provides the fastest achievable folding rate ($k^{\circ}_{MN} \approx 1.1 \times 10^7$ s^{-1}) for NCO→N folding process in the absence of barrier. Panel (c) also shows the pH-dependence of intrachains diffusion rates (transient binding of methionines, M65 and M80 (Δ) and histidines, H26 and H33 (∇)) measured following CO photolysis from base-unfolded Cyt-CO at pH ≥ 12.6 at 25 °C. In the denaturing milieu (pH > 12), the ln k_f began to increase and finally matches to the intrachains diffusion rates measured following CO photolysis from base-unfolded Cyt-CO at pH 12.6. At pH ~12.6, the microsecond folding for NCO→N conformational transition was best fitted to a bi-exponential rate expression and thus exhibits intrachains diffusive dynamics (transient binding of methionines, M65 and M80 (□) and histidines, H26 and H33 (•).

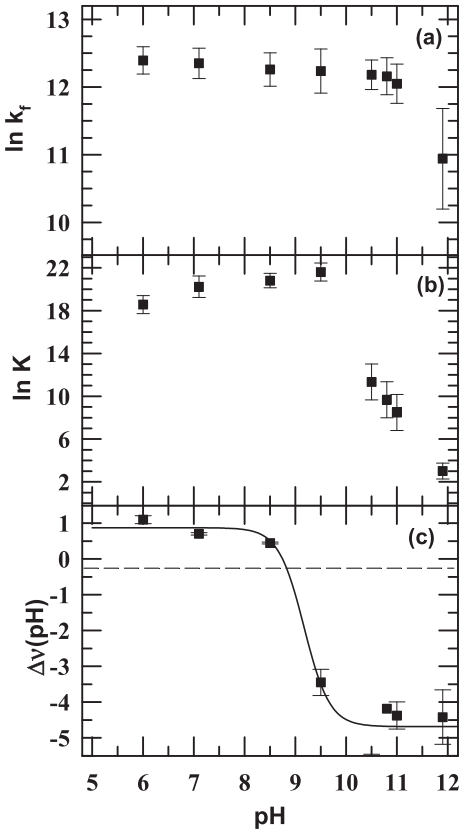

Fig. 6. Panels (a) and (b) show the variations of the ln k_f and ln *K* with pH. Between pH 7 and pH 11.9, there is very small change in the ln k_f (panel (a)) while within this range of pH, there is large change in the ln *K* (panel (b)). Panel (c) presents the variation of Δν (pH) with pH. At pH ~8.9, the Δν (pH) value is about zero, suggesting that there is no change in the number of bound proton upon unfolding. At pH ~6, the Δν (pH) value is about two, suggesting that two proton is taken up by protein upon unfolding. The lines through the data in panel (c) have been drawn by inspection only.

and pH 11.9 were obtained by differentiation of the ln *K* versus pH. Fig. 6c presents the variation of Δν (pH) as a function of pH. At pH ~8.9, the value of Δν (pH) was about zero, indicating that there was no change in the number of bound proton upon unfolding. At pH ~6, the value of Δν (pH) was about two, suggesting that two protons were taken up by protein upon unfolding.

4. Discussion

4.1. Cyt-CO is maximally stable at moderate alkaline pH

Relative to pH 7, ΔG_D° increases by ~2.1 kcal mol^{-1} at pH 9.5 (ΔG_D° is ~10.8 and ~12.9 kcal mol^{-1} at pH 7 and 9.5, respectively) (Fig. 1b and Table 1) which indicates that the favorable ionic interactions which stabilize Cyt-CO are increased at pH ~9.5. This result is consistent with an earlier report that showed yeast iso-2 ferricyt *c* has maximum stability between pH 9 and pH 10 [81]. The increase in stability of yeast iso-2 ferricyt *c* at alkaline pH was attributed to the pH-induced conformational change of protein [81]. An earlier report by Linderstrom-Lang [82] has revealed that the proteins have generally maximum stability at the pH near to isoelectric point (pI). The estimated pI of Cyt *c* is at pH ~10 which is very near to the pH where Cyt-CO has maximum thermodynamic stability (Fig. 1b). However, several other reports have revealed that many other proteins with acidic or basic pI are maximum stable near neutral pH [83,84]. These studies thus suggest that in addition to overall charges, other factors also play important roles in determining the folding energy of proteins. At relatively higher basic pH (pH > 10), the deprotonation of basic amino acid groups of Cyt-CO lead to unfavorable interactions amongst the negatively charged groups of protein which as a consequence subdue the alkaline pH-induced stabilization of Cyt-CO (Fig. 1b). Relative to pH 7, there is a large decrease in ΔG_D° of Cyt-CO at pH 11.9 (Fig. 1b and Table 1).

4.2. Cyt-CO unfolds via an intermediate

An earlier denaturant-induced equilibrium unfolding and kinetic study of Ferrocyt *c* in the presence of CO (≈1 mM) at pH 7.0 revealed that Cyt-CO unfolds *via* an intermediate [85]. A recent single-molecule and ensemble-averaged unfolding dynamics study of yeast iso-1-ferricyt *c* indicated that native yeast iso-1-ferricyt *c* unfolds through an intermediate with a native-like compactness

[86]. In an earlier study [53], the non-coincidence of far-UV CD (222 nm) and fluorescence-monitored alkaline pH-unfolding transitions of Ferricyt *c* is attributed due to the presence of an equilibrium intermediate. The absorbance (550 nm) and fluorescence-monitored alkaline pH-unfolding transitions of Cyt-CO in transition regions are not perfectly superimposable (Fig. 1d), which indicates accumulation of an equilibrium intermediate during the CO-induced unfolding of protein. However, it is not clear how the CO-induced unfolding of protein can do so.

4.3. The internal dynamics of Ferrocyt c is restricted in the subdenaturing limit of alkaline pH

NCO→N+CO and N+CO→NCO processes are typically Fe^{2+}−CO→Fe^{2+}−M80 and Fe^{2+}−M80→Fe^{2+}−CO displacement reactions, respectively, where the N- and NCO-states acquire energy required for CO association and dissociation by thermal fluctuations [51,52]. The M80-resident segment of the polypeptide, which is linked to the heme iron through the Fe^{2+}−M80 bond in N but is free in NCO, represents the partially unfolded Ω-loop formed between residues 70 and 85. The CO association and dissociation processes are expected to be controlled by the collective motion of M80-containing Ω-loop because (i) thermal factors for the neighboring residues of M80 are higher in the x-ray structure of cyt *c* [87], and (ii) intrinsic size and rigidity of ring system suppress the local mobility of heme ring [88]. An earlier 2D NMR investigation revealed the substantial perturbed residues during CO dissociation spans from residues 80 to 85 [85]. It is documented that CO association/dissociation kinetics can be monitored with the decay/rise of peak height at −3.26 ppm and other side resonances at pH 7, 22 °C [52]. Earlier reports by Bhuyan et al. have revealed that low-frequency local motions such as thermal collisions due to collective motional mode of the M80-contaning Ω-loop control the CO association and dissociation processes [51,52]. Thus, pH modulation of log $k_{ass/diss}$ in Fig. 2d reveals the manner by which the amplitudes of thermal-fluctuations responsible for CO association and dissociation vary in response to changing the pH of reaction medium. The decrease of log k_{ass} and log k_{diss} at pH ~9.8 and ~11, respectively (Fig. 2d) revealed that the amplitudes of thermal-fluctuations of the M80-contaning Ω-loop decreased in the subdenaturing limit of alkaline pH. This result provided the primary evidence that the internal dynamics of protein is restricted in the subdenaturing limit of alkaline pH. ^{1}H NMR spectra can also be used to evaluate the internal mobility and side chain environmental averaging of protein [89,90]. The NMR lines in ^{1}H NMR spectrum of NCO-state at pH 7 are narrow and well-dispersed (Fig. S1a). As pH is increased from 7 to 10.7, ^{1}H NMR spectrum of NCO-state appears to gain slightly more dispersion and sharpness of resonances all over the spectral width (Fig. S1b). This finding indicates that in the subdenaturing limit of alkaline pH, the internal protein interactions of NCO state are slightly increased. At relatively higher basic pH (pH ~13), NCO-state becomes denatured as shown by the loss of both chemical shift dispersion and line shape (Fig. S1c). The far-UV CD spectra of NCO state collected between pH 7 and pH 13 also revealed that NCO-state became denatured at higher basic pH (≥12.9) (Figs. S2a and S2b) while the secondary structure of NCO was stabilized in the subdenaturing limit of alkaline pH (≤11) (Fig. S2a and S2b).

If the amplitudes of thermal-fluctuations of protein or part of it are decreased in the subdenaturing limit of alkaline pH, the restricted thermal-fluctuations should slow down the speed of CO association and dissociation by increasing the activation energy barrier or activation enthalpy. Clearly, relative to pH 7, $\Delta H^{\ddagger}_{ass}$ and$\Delta H^{\ddagger}_{diss}$ are increased at pH 9.8 and 11, respectively (Tables 2 and 3). Furthermore, the increase of $\Delta H^{\ddagger}_{ass/diss}$ is also accompanied by a decrease in $-T\Delta S^{\ddagger}_{ass/diss}$ (Tables 2 and 3).

4.4. Rate rollover in the folding branch of chevron plot indicates that NCO→N folding proceed via at least one glassy state

Rate rollover in the folding branch is a specific characteristic of chevron plot for NCO→N conformational transition (Fig. 5c). Few earlier studies have shown that Cyt-CO exhibits rate rollover in the folding branch of chevron plot for UCO⇌NCOrefolding transition [47,48]. However, several other proteins such as CspB [91] and CI2 [92] do not show rate rollover in the folding branch of chevron plot. Several factors are likely to be responsible for rate rollover. If a protein has perfectly smooth energy landscape, it does not generally show rate rollover. In contrast, if a protein has rugged energy landscape, then it can show rate rollover. The pioneering work by Oliveberg and Silow has shown that the protein oligomerisation/aggregation can produce the rate rollover in the refolding arm [93]. The effect of varying protein concentration on the refolding kinetics can be used to determine whether the reaction is limited by aggregation or oligomerisation [94]. Between pH 7.0 and pH 10.5, the microsecond folding rates of NCO are not greatly changed with varying the protein concentration from 25 to 50 μM. However, at low protein concentrations (≤15 μM), the signal-to-noise ratio in the post CO photolysis microsecond folding kinetic trace data (550 nm) of NCO is very poor to analyze the data. Based on these observations, it is difficult to ascertain whether the rollover in the refolding arm is occurred due to protein oligomerisation/aggregation. Chan and coworkers have reported that rate rollover in the chevron plot is due to kinetic traps under native-like conditions [95,96]. Under native-like conditions, the internal frictional effects could also cause rate rollover in the folding chevron [49,95–98]. Within the formalism of classical kinetics, Roder and coworkers have expounded that rate rollover occurs due to trapping of structural intermediate [99]. One more possible reason for rate rollover is a broad energy barrier because it can separate native state from initial state [100]. These different explanations thus reveal that the roughness at the bottom of funnel is the major cause of slowing down the folding. Several factors such as accumulation of one or more structural intermediate, kinetic traps set up by non-native interactions and the internal frictional effects contribute to the roughness [49,95–98,101,102]. These observations thus reveal that rate rollover in the folding branch of chevron plot for NCO→N conformational transition attributes at least one kinetic trap intermediate, I (NCO⇌I⇌N) that occupies an energy well. At higher pH (≥11), the intermediate, I is indeed destabilized and the pH function of ln k_f is linear.

In accordance of landscape theory, once the folding ensemble has passed from the MG-like band over the transition state region of the funnel, the folding is then dominated by glassy dynamics [103–105]. Glass transitions are generally typified by stretched exponentials [106]. According to few previous studies, the finding of non single-exponential relaxation during folding has been attributed to glassy dynamics behavior of proteins [107,108]. However, under strongly native-like conditions, the simple single exponential kinetics also exhibits rate rollover due to kinetic trapping and glassy dynamics [95]. In this perspective, rate rollover in Fig. 5c (pH ≤ 11) suggests kinetic trapping and a glass transition of NCO en route to N.

4.5. Quantitative estimation of the pH-dependant ionic interactions in the stability and transition state for folding of Cyt-CO

The relative changes in the apparent free energy of folding ($\Delta\Delta G^{\circ}(pH_2, pH_1)$) and activation folding energy ($\Delta\Delta G^{\circ\ddagger}(pH_2, pH_1)$) of protein at a pH relative to the initial state can be calculated form eqs (6) and (7), respectively [9,21],

$$\Delta\Delta G^{\circ}(\mathrm{pH}_2,\mathrm{pH}_1) = \Delta G^{\circ}(\mathrm{pH}_2) - \Delta G^{\circ}(\mathrm{pH}_1) = 2.303RT \int_{\mathrm{pH}_1}^{\mathrm{pH}_2} \Delta\nu(\mathrm{pH})d\mathrm{pH} \quad (6)$$

$$\Delta\Delta G^{\circ\ddagger}(\mathrm{pH}_2,\mathrm{pH}_1) = \Delta G^{\circ\ddagger}(\mathrm{pH}_2) - \Delta G^{\circ\ddagger}(\mathrm{pH}_1) = 2.303RT \int_{\mathrm{pH}_1}^{\mathrm{pH}_2} \Delta\nu^{\ddagger}(\mathrm{pH})d\mathrm{pH} \quad (7)$$

The quantitative development of electrostatic interactions in the transition state for folding can be measured by determining the ratio [9–11,21],

$$\beta^{\mathrm{pH}} = \int_{\mathrm{pH}_1}^{\mathrm{pH}_2} \Delta\nu^{\ddagger}(\mathrm{pH})\mathrm{dpH} \Big/ \int_{\mathrm{pH}_1}^{\mathrm{pH}_2} \Delta\nu(\mathrm{pH})\mathrm{dpH} \quad (8)$$

$$\beta^{\mathrm{pH}} = \left[\ln k_f(\mathrm{pH}_2) - \ln k_f(\mathrm{pH}_1)\right] \Big/ \left[\ln K(\mathrm{pH}_2) - \ln K(\mathrm{pH}_1)\right] \quad (9)$$

Relative to pH 7, the β^{pH} at different pH, ranging from pH 6 to pH 11.9 were estimated by using eq (9). The β^{pH} thus estimated between pH 6 and pH 11.9 for both microsecond and millisecond folding were less than by 0.15 (Table 4). There are few other studies which estimated the β^{pH} or $\Delta\nu^{\ddagger}(\mathrm{pH})/\Delta\nu(\mathrm{pH})$ ratio for other proteins (barnase [40], CTNL9 [11], NTL9 [9], and CI-2 [39]). It is interesting to compare the current results with those pH-dependent folding studies. The estimated β^{pH} for barnase [40], CTL9 [11], CI-2 [39], and NTL9 [9] were ~0.5, ~0.6, ~0.25 and ~0.3, respectively. The larger β^{pH} for barnase (~0.5) and CTNL9 (~0.6) were attributed to a better development of electrostatic interactions in the transition states for folding of these two proteins [11,40]. On the other hand, the smaller β^{pH} for CI-2 (~0.25) and NTL9 (~0.3) were attributed to a weaker development of electrostatic interactions in the transition states for folding of CI-2 and NTL9 [9,39]. In the present study, the estimated β^{pH} for Cyt-CO between pH 6 and pH 11.9 was noticeably smaller ($\leq$0.15) which revealed that the electrostatic interactions were very poorly developed in the transition state for folding of Cyt-CO.

5. Conclusions

Thermodynamic analysis of urea-induced equilibrium unfolding transitions measured between pH 6 and pH 11.9 revealed that Cyt-CO has maximum thermodynamic stability at alkaline pH ~9.5 with a value of $\Delta G_D^{\circ} \approx 12.9$ kcal mol^{-1}. Unfolded Cyt-CO in refolding buffer refolds rapidly to a native-like NCO-state. Collective motions of the Ω-loop control the thermally-driven CO dissociation from NCO-state and association to N-state. Analysis of the pH-dependent rate coefficients of CO association and dissociation reactions revealed that the thermal motion of the Ω-loop first decreased in the subdenaturing limit of alkaline pH and then increased as the protein was taken from subdenaturing to denaturing milieu. Laser photolysis of the Fe^{2+}-CO bond in NCO-state triggered folding of NCO to N-state. The microsecond folding rate for NCO→N conformational transition was measured all across the alkaline pH-unfolding transitions of protein, which produced the rate rolls over in the folding branch of chevron plot (pH ≤ 11), indicating that NCO→N folding proceeds *via* at least one glassy state. Between pH 7 and 11.9, the ln k_f decreased by < 1.5 units, while the ln K decreased by ~11.8 units. This comparison suggests that the pH-dependent ionic interactions contributed significantly to the thermodynamic stability of protein but had a small effect on the CO photolysis-triggered microsecond folding kinetics of NCO. By using the classic W-T linkage relation, the β^{pH} for microsecond and millisecond folding of cyt-CO were estimated between pH 6 and 11.9, which were less than by 0.15, indicating that the electrostatic interactions were weakly formed in the transition states for microsecond and millisecond folding of Cyt-CO.

Table 4
pH-dependence of the ln k_f, ln K, Δν (pH) and β^{pH} for cyt-CO.

pH	ln k_f (s^{-1})	ln K	Δν(pH)	β^{pH}	pH	ln k_f (s^{-1})	ln K	Δν(pH)	β^{pH}
6.0	12.39	15.6	2.6	−0.02	10.5	12.18	14.8	−7.9	0.05
7.0	12.35	18.2	1.9	−0.19	10.8	12.16	12.1	−9.0	0.03
8.0	12.26	20.1	1.4	−0.05	11.0	12.05	10.3	−6.7	0.04
9.5	12.24	21.6	−2.6	−0.03	11.9	10.94	6.4	−4.4	0.12

Acknowledgements

This work was supported by the UGC Major Research grant (to R.K. (F. no. 41-258/2012 (SR)), Council of Scientific and Industrial Research Grant (to R.K. No. 37(148s)/1r/EMR -II), and Department of Science and Technology SERB Research Grant (to R.K., File NO. EMR/2014/000242), Department of Biotechnology Research Grant (to R.K., No. BT/PR11684/BRB/10/1300/2014), and Indian Council of Medical Research Grant (to R.K., NO. 52/6/2013-BMS), Government of India. I gratefully acknowledge many helpful suggestions and support of Prof. Abani K Bhuyan.

Appendix A. Supplementary data

Supplementary data related to this article can be found at http://dx.doi.org/10.1016/j.abb.2016.07.010.

References

[1] A. Karshikoff, R. Ladenstein, in: V.N. Uversky, E. Permyakov (Eds.), Methods in Protein Structure and Stability Analysis: Conformational Stbility, Size, Shape and Surface of Protein Molecules, Nova Biomedical Books, New York, 2007, pp. 71–107.
[2] D. Perl, G. Holtermann, F.X. Schmid, Biochemistry 40 (2001), 15501–25011.
[3] B.N. Dominy, D. Perl, F.X. Schmid, C.L. Brooks 3rd, J. Mol. Biol. 319 (2002) 541–554.
[4] R. Jaenicke, G. Bohm, Curr. Opin. Struct. Biol. 8 (1998) 738–748.
[5] C.N. Pace, Methods Enzymol. 259 (1995) 538–554.
[6] G. Vogt, S. Woell, P. Argos, J. Mol. Biol. 269 (1997) 631–643.
[7] A.H. Elcock, J.A. McCammon, J. Mol. Biol. 280 (1998) 731–748.
[8] M.P. Perutz, Science 201 (1978) 1187–1191.
[9] D.L. Luisi, D.P. Raleigh, J. Mol. Biol. 299 (2000) 1091–1100.
[10] J.C. Horng, J.H. Cho, D.P. Raleigh, J. Mol. Biol. 345 (2005) 163–173.
[11] S. Satoshi, D.P. Raleigh, J. Mol. Biol. 318 (2002) 571–582.
[12] Z.S. Hendsch, B. Tidor, Protein Sci. 3 (1994) 211–226.
[13] D.J. Barlow, J.M. Thornton, J. Mol. Biol. 168 (1983), 867–865.
[14] S. Kumar, R. Nussivov, J. Mol. Biol. 293 (1999) 1241–1255.
[15] B. Honig, A. Nicholls, Science 268 (1995) 1144–1149.
[16] S.R. Campos, M. Machuqueiro, A.M. Baptista, J. Phys. Chem. B 7 (2010) 12692–12700.
[17] D. Vila-Viçosa, S.R. Campos, A.M. Baptista, M. Machuqueiro, J. Phys. Chem. B 116 (2012) 8812–8821.
[18] T.C. Bjorndahl, G.P. Zhou, X. Liu, R. Perez-Pineiro, V. Semenchenko, F. Saleem, S. Acharya, A. Bujold, C.A. Sobsey, D.S. Wishart, Biochemistry 50 (2011) 1162–1173.
[19] E. Durr, I. Jelesarov, H.R. Bosshard, Biochemistry 38 (1999) 870–880.
[20] D. Bashford, M. Karplus, Biochemistry 29 (1990) 10219–10225.
[21] A.S. Yang, B. Honig, J. Mol. Biol. 231 (1993) 459–474.
[22] C.A. Blasie, J.M. Berg, Biochemistry 36 (1997) 6218–6222.
[23] M.K. Gilson, A. Rashin, R. Fine, B.H. Honig, J. Mol. Biol. 183 (1995) 503–516.
[24] B. Ibarra-Molero, V.V. Loladze, G.I. Makhatadze, J.M. Sanchez-Ruiz, Biochemistry 38 (1999) 8138–8149.
[25] A. Horovitz, L. Serrano, B. Avron, M. Bycroft, A.R. Fersht, J. Mol. Biol. 216 (1990) 1031–1044.
[26] K.J. Lumb, P.S. Kim, Science 268 (1995) 436–439.
[27] C.N. Pace, D.V. Laurents, J.A. Thomson, Biochemistry 29 (1990) 2564–2572.
[28] D. Sali, M. Bycroft, A.R. Fersht, J. Mol. Biol. 220 (1991) 779–788.
[29] W. Shaller, A.D. Robertson, Biochemistry 34 (1995) 4714–4723.

[30] S. Spector, M. Wang, S.A. Carp, J. Robblee, Z.S. Hendsch, R. Fairman, B. Tidor, D.P. Raleigh, Biochemistry 39 (2000) 872–879.
[31] W.D. Kohn, C.M. Kay, R.S. Hodges, J. Mol. Biol. 267 (1997) 1039–1052.
[32] P. Strop, S.L. Mayo, Biochemistry 39 (2000) 1251–1255.
[33] C.D. Waldburger, J.F. Schildbach, R.T. Sauer, Nat. Struct. Biol. 2 (1995) 122–128.
[34] Y.J. Tan, M. Oliveberg, B. Davis, A.R. Fersht, J. Mol. Biol. 254 (1995) 980–992.
[35] M. Oliveberg, V.L. Arcus, A.R. Fersht, Biochemistry 34 (1995) 9424–9433.
[36] S. Cavagnero, D.A. Debe, Z.H. Zhou, M.W.W. Adams, S.I. Chan, Biochemistry 37 (1998) 3369–3376.
[37] L. López-Arenas, S. Solís-Mendiola, A. Hernàndez-Arana, Biochemistry 38 (1999) 15936–15944.
[38] R. Jain, R. Kumar, S. Kumar, R. Chhabra, M.C. Agarwal, Arch. Biochem. Biophys. 585 (2015) 52–63.
[39] Y.-J. Tan, M. Oliveberg, A.R. Fersht, J. Mol. Biol. 264 (1996) 377–389.
[40] A.C. Tissot, S. Vuilleumier, A.R. Fersht, Biochemistry 35 (1996) 6786–6794.
[41] M. Xu, O. Beresneva, R. Rosario, H. Roder, J. Phys. Chem. B 116 (2012) 7014–7025.
[42] R. Jain, S. Kaur, R. Kumar, J. Biochem. 153 (2013) 161–177.
[43] P. Nicholls, Biochim. Biophys. Acta 346 (1974) 261–310.
[44] H. Pellitier, J. Kraut, Science 258 (1992) 1748–1755.
[45] C. Kawai, F.M. Prado, G.L. Nunes, P. Di Mascio, A.M. Carmona-Ribeiro, I.L. Nantes, J. Biol. Chem. 280 (2005) 34709–34717.
[46] G.R. Moore, G.W. Pettigrew, Cytochrome c: Evolutionary, Structural and 700 Physiochemical Aspects, Springer-Verlag, Berlin, 1990.
[47] A.K. Bhuyan, R. Kumar, Biochemistry 41 (2002) 12821–12834.
[48] R. Kumar, A.K. Bhuyan, J. Phys. Chem. B 112 (2008) 12549–12554.
[49] S.A. Pabit, H. Roder, S.J. Hagen, Biochemistry 43 (2004) 12532–12538.
[50] M. Yadaiah, R. Kumar, A.K. Bhuyan, Biochemistry 46 (2007) 2545–2551.
[51] A.K. Bhuyan, Biochemistry 41 (2002) 13386–13394.
[52] R. Kumar, N.P. Prabhu, M. Yadaiah, A.K. Bhuyan, Biophys. J. 87 (2004) 2656–2662.
[53] R. Kumar, N.P. Prabhu, D.K. Rao, A.K. Bhuyan, J. Mol. Biol. 364 (2006) 483–495.
[54] J.M. Vanderkooi, M. Erecinska, Eur. J. Biochem. 60 (1975) 199–207.
[55] T.,Y. Tsong, J. Biol. Chem. 249 (1974) 1988–1990.
[56] M. Santoro, D.W. Bolen, Biochemistry 27 (1988) 8063–8068.
[57] D.K. Rao, R. Kumar, M. Yadaiah, A.K. Bhuyan, Biochemistry 45 (2006) 3412–3420.
[58] A.K. Bhuyan, D.K. Rao, N.P. Prabhu, Biochemistry 44 (2005) 3034–3040.
[59] R. Jain, D. Sharma, S. Kumar, R. Kumar, Biochemistry 53 (2014) 5221–5235.
[60] U. Mayor, N.R. Guydosh, C.M. Johnson, J.G. Grossman, S. Sato, G.S. Jas, S.M.V. Freund, D.O.V. Alonso, V. Daggett, A.R. Fersht, Nature 421 (2003) 863–867.
[61] R.M. Ballew, J. Sabelko, M. Gruebele, Proc. Natl. Acad. Sci. U. S. A. 93 (1996) 5759–5764.
[62] R. Kumar, N.P. Prabhu, A.K. Bhuyan, Biochemistry 44 (2005) 9359–9367.
[63] J. Choi, Y.O. Jung, J.H. Lee, C. Yang, B. Kim, H. Ihee, Chem. Phys. Chem. 9 (2008) 2708–2714.
[64] C.M. Jones, E.R. Henry, Y. Hu, C.K. Chan, S. Luck, A.K. Bhuyan, H. Roder, J. Hofrichter, W.A. Eaton, Proc. Natl. Acad. Sci. U. S. A. 90 (1993) 11860–11864.
[65] S.J. Hagen, C.W. Carswell, E.W. Sjolander, J. Mol, Biol. 305 (2001) 1161–1171.
[66] S.J. Hagen, J. Hofrichter, A. Szabo, W.A. Eaton, Proc. Natl. Acad. Sci. U. S. A. 93 (1996) 11615–11617.
[67] R.M. Ballew, J. Sabelko, M. Gruebele, Nat. Struct. Biol. 3 (1996) 923–936.
[68] R.M. Ballew, J. Sabelko, M. Gruebele, Proc. Natl. Acad. Sci. U. S. A. 93 (1996) 5759–5764.
[69] B.I. Greene, R.M. Hochstrasser, R.B. Weisman, W.A. Eaton, Proc. Natl. Acad. Sci. U. S. A. 75 (1978) 5255–5259.
[70] D.A. Chernoff, R.M. Hochstrasser, A.W. Steele, Proc. Natl. Acad. Sci. U. S. A. 77 (1980) 5606–5610.
[71] J. Terner, J.D. Stong, T.G. Spiro, M. Nagumo, M. Nicol, M.A. El-Sayed, Proc. Natl. Acad. Sci. U. S. A. 78 (1981) 1313–1317.
[72] J. Terner, T.G. Spiro, M. Nagumo, M. Nicol, M.A. El-Sayed, J. Am. Chem. Soc. 102 (1981) 3238–3239.
[73] E.W. Findsen, J.M. Friedman, M.R. Ondrias, S.R. Simon, Science 229 (1985) 661–665.
[74] L.P. Murray, J. Hofrichter, E.R. Henry, W.A. Eaton, Biophys. Chem. 29 (1988) 63–76.
[75] S. Williams, T.P. Causgrove, R. Gilmanshin, K.S. Fang, R.H. Callender, W.H. Woodruff, R.B. Dyer, Biochemistry 35 (1996) 691–697.
[76] I.K. Lednev, A.S. Karnoup, M.C. Sparrow, S.A. Asher, J. Am. Chem. Soc. 121 (1999) 8074–8086.
[77] P.A. Thompson, W.A. Eaton, J. Hofrichter, Biochemistry 36 (1997) 9200–9210.
[78] W.A. Eaton, V. Munoz, P.A. Thompson, E.R. Henry, J. Hofrichter, Acc. Chem. Res. 31 (1998) 745–753.
[79] J. Wyman Jr., Adv. Protein Chem. 16 (1964) 223–286.
[80] C. Tanford, Ad. Protein Chem. 24 (1970) 1–95.
[81] J.J. Osterhout Jr., K. Muthukrishnan, B.T. Nall, Biochemistry 24 (1985) 6680–6694.
[82] C.R. Linderstrom-Lang, Compt. Rend. Trav. Lab. Carlsb. Ser. Chim. 15 (1924) 1–29.
[83] D.E. Anderson, W.J. Becktel, F.W. Dahlquist, Biochemistry 29 (1990) 2403–2408.
[84] S. Venkataramani, J. Truntzer, D.R. Coleman, J. Pharm. Bioallied. Sci. 5 (2013) 148–153.
[85] R.F. Latypov, K. Maki, H. Cheng, S.D. Luck, H. Roder, J. Mol. Biol. 383 (2008) 437–453.
[86] J. Choi, S. Kim, T. Tachikawa, M. Fujitsuka, T. Majima, Phys. Chem. Chem. Phys. 13 (2011) 5651–5658.
[87] A.M. Berghuis, G.D. Brayer, J. Mol. Biol. 223 (1992) 959–976.
[88] J.D. Morgan, J.A. McCammon, Biopolymers 22 (1983) 1579–1593, 734.
[89] M. Ohgushi, A. Wada, FEBS Lett. 164 (1983) 21–24.
[90] O.B. Ptitsyn, J. Protein Chem. 6 (1987) 273–293.
[91] T. Schindler, M. Herrler, M.A. Marahiel, F.X. Schmid, Nat. Struct. Biol. 2 (1995) 663–673.
[92] S.E. Jackson, A.R. Fersht, Biochemistry 30 (1991) 10428–10435.
[93] M. Silow, M. Oliveberg, Proc. Natl. Acad. Sci. U. S. A. 94 (1997) 6084–6086.
[94] N.D. Werbeck, P.J. Rowling, V.R. Chellamuthu, L.S. Itzhaki, Proc. Natl. Acad. Sci. U. S. A. 105 (2008) 9982–9998.
[95] H. Kaya, H.S. Chan, J. Mol. Biol. 315 (2002) 899–909.
[96] H. Kaya, H.S. Chan, J. Mol. Biol. 326 (2002) 911–931.
[97] H.S. Chan, S. Shimizu, H. Kaya, Methods Enzymol. 380 (2004) 350–379.
[98] H.S. Chan, T. Chen, Phys. Chem. Chem. Phys. 16 (2014) 6460–6479.
[99] S. Khorasanizadeh, I.D. Peters, H. Roder, Nat. Struct. Biol. 3 (1996) 193–205.
[100] D.E. Otzen, O. Kristensen, M. Proctor, M. Oliveberg, Biochemistry 38 (1999) 6499–6511.
[101] Y. Bai, T.R. Sosnick, L. Mayne, S.W. Englander, Science 269 (1995) 192–197.
[102] L. Hoang, S. Bédard, M.M.G. Krishna, Y. Lin, S.W. Englander, Proc. Natl. Acad. Sci. U. S. A. 99 (2002) 12173–12178.
[103] J.D. Bryngelson, P.G. Wolynes, Proc. Natl. Acad. Sci. U. S. A. 84 (1987) 7524–7528.
[104] P.G. Wolynes, J.N. Onuchic, D. Thirumalai, Science 267 (1995) 1619–1620.
[105] J.D. Bryngelson, J.N. Onuchic, N.D. Socci, P.G. Wolynes, Proteins 21 (1995) 167–195.
[106] C.A. Angell, Science 267 (1995) 1924–1935.
[107] L.A. Morozova-Roche, J.A. Jones, W. Noppe, C.M. Dobson, J. Mol. Biol. 289 (1999) 1055–1073.
[108] D.T. Leeson, F. Gai, H.M. Rodrigues, L.M. Gregoret, R.B. Dyer, Proc. Natl. Acad. Sci. U. S. A. 97 (2000), 2527–2732.